

*Author Version :International Journal of Climatology, vol.38(2); 2018; 1074-1086*

## **Processes controlling the accelerated-warming of the Arabian Sea**

**Joshua Rosario D'Mello<sup>†</sup> and S. Prasanna Kumar\***

CSIR- National Institute of Oceanography, Dona Paula- 403 004, Goa, India.

\*Corresponding author

email: [prasanna@nio.org](mailto:prasanna@nio.org)

Telephone: 91-832-2450300

Fax: 91-832-2450608

<sup>†</sup> Presently at Rosary College of Commerce and Arts, Navelim- 403 707, Salcete, Goa.

**Running Title:** Arabian Sea rapid-warming processes

### **Key points**

- Accelerated-warming of the Arabian Sea after-1995
- Decreased cooling due to reduced summer-upwelling and winter convective-mixing
- Increasing humidity, reducing wind-speed and evaporation trends cause SST-rise

### **Abstract**

The Arabian Sea (AS) has undergone a regime shift after 1995, manifesting the disruption of its natural decadal-cycle over-riding a secular rise in its sea surface temperature (SST). Using a suite of in-situ and remote sensing data we show that the rate of post-1995 accelerated-warming is spatially different, due to regionally and seasonally differing oceanographic processes. Along parts of the western-boundary, the accelerated-warming was mediated by a reduction in the post-1995 linear trend of wind-speed during summer-monsoon leading to reduced upwelling and also reduced evaporation trend. In the northeast AS, post-1995 increase in specific humidity during late-winter, lead to a decrease in the evaporative-cooling and subsequent convective-mixing resulting in the increased rate of warming. The continued warming seen in the northeast AS until spring inter monsoon was due to the increasing net heat flux trend into the ocean along with reducing-trend in evaporation. The accelerated-warming in the central AS was linked to the reduced wind-speed trend.

**Key words:** Sea surface temperature (SST), warming-trend, reduced-cooling, Arabian Sea, upwelling, winter cooling, decadal-cycle

## 1. Introduction

The Arabian Sea (AS) is a tropical-basin situated in the western part of the north Indian Ocean. The distinct feature of this basin is that it is land-locked in the north at approximately 25°N latitude and comes under the monsoon regime. As a result of being blocked by the Eurasian landmass, the basin's waters are not cooled by the polar-waters from the north, while the monsoons lead to a strong seasonality in the hydrography and circulation. The semi-annual wind-reversal associated with monsoons, having southwesterly winds during summer-monsoon (June to September) and northeasterly winds during winter-monsoon (November to February), leads to a reversal in the direction of surface current as well. The winds during spring (March to May) and fall (October) intermonsoons are weak and variable. The waters of the basin also experiences cooling twice-annually in summer and winter-monsoons. During summer-monsoon upwelling of cold sub-surface waters along Somalia (Smith and Codispoti, 1980), Arabia (Smith and Bottero, 1977) and the southern part of the west-coast of India (Sharma, 1966; Varadachari and Sharma, 1967) cools the surface waters. However, in the east-central AS the summer-cooling was attributed to the downward transfer of heat due to mixing of warmer surface and the colder sub-surface waters (Ramesh Babu and Sastry, 1984). In addition, the open-ocean upwelling driven by positive wind-stress curl (Bauer *et al.*, 1991) north of the Findlater Jet (Findlater, 1969) as well as wind-mixing contributes to the cooling of various regions in the AS during summer-monsoon (Prasanna Kumar *et al.*, 2001). In winter, the upper layers of the northern AS are cooled by the radiative heat loss combined with evaporative-cooling and subsequent convective-mixing (Prasanna Kumar and Prasad, 1996). Based on mooring data Weller *et al.* (2002) showed that during the winter, in the period from October 1994 to October 1995, under the influence of dry and moderate winds and clear skies when the SST dropped by around 3°C, the ocean lost 19.7 W/m<sup>2</sup> and the mixed-layer deepened by 100 m in the central AS. Meso-scale eddies and heat-budgets were studied by Fischer *et al.* (2002), while the influences of the diurnal and intra-seasonal forcing on the mixed-layer and biological variability in the central AS were studied by McCreary *et al.* (2001).

On an inter-annual time scale De Boyer Montégut *et al.* (2007) showed that the eastern AS SST is strongly controlled by winds, through variation in the latent heat fluxes, while the western AS SST is controlled by vertical processes and horizontal advection.

Recent studies on the AS SST are indicating a secular warming-trend. It was RupaKumar *et al.* (2002) who first documented the rise in sea surface temperature (SST) of the AS, during the period

from 1904 to 1994, which was  $0.5^{\circ}\text{C}$ . Subsequently, the study by Alory *et al.* (2007), based on 1960 to 1999 thermal data from Indian Ocean, showed a warming of around  $1^{\circ}\text{C}$  over large regions in the AS. Prasanna Kumar *et al.* (2009) noted that the AS is experiencing secular-warming and undergoing a regime shift after 1995 as seen from the disruption in the natural decadal-cycle of the SST. The heat-content of the upper-ocean, in the Indian Ocean, shows a warming-trend and the Hadley Centre Sea Ice and SST show that the tropical Indian Ocean regions warmed faster than most of the tropical Pacific and Atlantic, since the 1950s (see Han *et al.*, 2014 and references therein). Roxy *et al.* (2014) showed that the western tropical Indian Ocean is warming faster than the rest of the tropical oceans, while Dinesh Kumar *et al.* (2016) reported an increasing SST of  $0.12^{\circ}\text{C}/\text{decade}$  in the AS for the period from 1960 to 2009. Han *et al.* (2014) reviewed the decadal variability and the long term-trends in the Indian Ocean. Though it is unequivocally evident from the above that the AS is indeed undergoing a secular-warming, it is not known whether the reported warming-trends will be similar in all parts of the AS. Hence, the present study attempts to understand the nature and characteristics of this warming in different parts of the AS and at understanding the processes that controls such warming.

## 2. Data and Methodology

The data pertaining to SST, specific humidity, surface wind components were obtained from the International Comprehensive Ocean-Atmosphere Data Set (ICOADS) (Woodruff *et al.*, 2011). To our best knowledge, ICOADS is the most complete and heterogeneous collection of surface marine-data. There are some data-coverage issues though, a cause being no addition of delayed-mode ship data in recent years. The ship-recorded data dominate until 1970s; thereafter contribution of buoys and other automated platforms has rapidly increased. Ship-recorded data are mainly in the shipping lanes. Drifting buoys data have near ubiquitous coverage, but as they are generally not recovered, the recording sensors may drift which results in a reduced accuracy. Some other problems of ICOADS data are the change in observation practices, i.e. bucket-intake and engine-intake. This was sorted out to some extent in HADSST (Rayner *et al.*, 2003, Rayner *et al.*, 2006, Kennedy *et al.*, 2011a; Kennedy *et al.*, 2011b). The sampling of ICOADS is another issue. However this was addressed for all ICOADS variables (Gulev *et al.*, 2007a; Gulev *et al.*, 2007b). Supplementary figures 1, 2 and 3 are given to show more information on the quality of the ICOADS SST data. Despite a number of drawbacks, due to the widely differing data-source, ICOADS data is used as the basis for many derived products and is regarded as the long-term marine-surface reference data-set (Woodruff *et al.*,

2011). In order to examine the robustness of the ICOADS data in the Arabian Sea, we have plotted the basin-averaged 60-month running mean ICOADS SST, NOAA Optimally Interpolated SST (<https://www.esrl.noaa.gov/psd/data/gridded/data.noaa.oisst.v2.html>) and Kaplan SSTA ([https://www.esrl.noaa.gov/psd/data/gridded/data.kaplan\\_sst.html](https://www.esrl.noaa.gov/psd/data/gridded/data.kaplan_sst.html)) in the supplementary figure 4. From the figure it is evident that though there are differences between data sets, all of them showed similar trend. Hence, for the present study we principally relied upon the ICOADS and the values were extracted for the AS in the domain equator to 25°N and 45°E to 80°E. The evaporation rate was taken from Objectively Analyzed Air-Sea Fluxes (OAFlux). The OAFlux data uses optimal blending of satellite retrievals and three atmospheric re-analyses (Yu *et al.*, 2008). The precipitation data are the CDC Derived NCEP Reanalysis Products Surface Flux. The evaporation and precipitation difference (E-P) were then computed, using the above-mentioned data-sets. The Arabian Sea as a whole is generally dominated by evaporation; but in-order to better represent the freshwater flux, E-P is taken. The monthly gridded data of the shortwave radiation, longwave radiation (LWR), latent heat flux (LHF) and sensible heat flux (SHF) are from the NCEP/NCAR reanalysis monthly means and other derived variables data (Kalnay *et al.*, 1996). The NCEP/NCAR reanalysis data are classified into four types, based on the influence of observations and the model. The variables of class “A” are influenced strongly by the observations and are more reliable. The flux data are of class “C” which are variables not directly affected by observations. Although the classification is somewhat subjective, a little caution is required in interpreting the results of the re-analysis variables of class “C” (Kalnay *et al.*, 1996). There have been some studies showing the over-estimation or underestimation of fluxes in the NCEP/ NCAR data as seen by the studies of Josey (2001) in the Atlantic Ocean and Moore and Renfrew (2002), Kubota et al. (2008) in the Pacific Ocean. The NCEP/NCAR large SHF and LHF overestimation compared to World Ocean Circulation Experiment (WOCE) ships was studied by Smith et al. (2001). However, in the absence of large continuously-observed flux data, this reanalysis-data is probably the best alternative, and besides this the Tropflux and OAFlux data are of shorter periods. The NCEP/NCAR flux data were used to compute the net heat flux (NHF). All fluxes are considered positive into the ocean. The TropFlux data, which is not used in this analysis, is a project aimed giving heat and momentum flux data at daily interval, in the region from 30°N to 30°S. The data is available only in the period from 1979 to 2013 March. The international sunspot number data are produced by the Solar Influences Data Analysis Center (SIDC), World Data Center for the Sunspot Index, at the Royal Observatory of Belgium. The Carbon dioxide concentration values, on Mauna Loa, from 1958 March to 2012 September and globally from

1980 January to 2012 August annually, are obtained from [ftp://ftp.cmdl.noaa.gov/ccg/co2/trends/co2\\_mm\\_mlo.txt](ftp://ftp.cmdl.noaa.gov/ccg/co2/trends/co2_mm_mlo.txt) and [ftp://ftp.cmdl.noaa.gov/ccg/co2/trends/co2\\_mm\\_gl.txt](ftp://ftp.cmdl.noaa.gov/ccg/co2/trends/co2_mm_gl.txt) respectively. The Carbon dioxide concentrations at Mauna Loa are merged to the global Carbon dioxide concentration data to extend the time series before 1980 January (Keeling *et al.*, 2001; Keeling *et al.*, 2005).

The temperature section is plotted using from Simple Ocean Data Assimilation (SODA) data v2.2.4. The data used and its characteristics are mentioned in the Table 1.

All the data were analysed and plotted using ferret software, in the time period from 1960 January to 2011 December, wherever available. The data period was divided at 1995 November as it is the minimum of a sunspot-number cycle period and there are differences in SST decadal-cycle and slopes across this period. The 60-month running-means were computed for the parameters, besides computing the slopes of the trendlines and their correlation coefficients with SST, both the fore-mentioned at 95% significance levels, in the pre-1995 November and post-1995 November periods. The non-zero slopes of the trend lines were computed (<http://stattrek.com/regression/slope-test.aspx?Tutorial=AP>). The basin-averaged 60-month running mean SST slopes were found to be significant with p-value <0.0001.

### **3. Results and discussion**

We first examined the trend in the basin-averaged SST in the context of sunspot-number cycle and the atmospheric carbon dioxide concentrations during 1960 to 2011, in order to study the differential-rate of warming across-1995. Subsequently, we explored how the warming-rate seen in the SST differs regionally and the parameters responsible for it. Finally, we investigated the processes that led to the observed differential-warming in the AS.

#### **3.1 Basin-averaged SST, sunspot-number cycle and atmospheric CO<sub>2</sub> concentration**

The sunspot number 60-month running-mean shows the 11-year cycle (Figure 1), first discovered by Schwabe and Schwabe Herrn (1844). This 11-year solar cycle is also seen in its luminosity (Willson and Hudson, 1991). Variations in the solar-luminosity (total energy-output) are caused by the changing sunspot-numbers, during the 11-year cycle (Foukal *et al.*, 2006). The solar-irradiance affects the climate (Haigh *et al.*, 2010) and sunspot number is taken as a proxy for the solar-irradiance. The basin-averaged 60-month running-mean SST in the AS, in the period from 1960 January to 2011 December, showed a gradual increasing-trend, at the rate of 0.010°C/year, which was overriding the dominant decadal-cycle (Figure 1). White *et al.* (1997) showed that the natural

decadal-cycle is closely linked to the solar activity. A noteworthy feature was the co-variation of AS SST and sunspot-number cycle until 1995 demonstrating the dominant decadal-cyclicity, a result consistent with Prasanna Kumar *et al.* (2009). Such a link between the decadal-cycle and SST is also seen in the eastern part of the North Indian Ocean i.e. the Bay of Bengal, from 1960 to 1995 (D'Mello and Prasanna Kumar, 2015). However, this decadal relation between Arabian Sea SST and sunspot-number cycle is disrupted post-1995, as can be seen in figure 1. As November 1995 is the minimum of the sunspot number, it is chosen as the time to divide the time series into two periods. The rate of warming, as inferred from the slope of the SST, increased from  $0.008^{\circ}\text{C}/\text{year}$  in the pre-1995 period to  $0.014^{\circ}\text{C}/\text{year}$  in the post-1995 period, a result not reported in Prasanna Kumar *et al.* (2009). However the changes in the total energy-output of the sun is unlikely to have any significant impact on the global-warming since the seventeenth-century (Foukal *et al.*, 2006). The increasing SST-trend is due to the increasing  $\text{CO}_2$  concentration, through greenhouse effect (Arrhenius, 1896). However the  $\text{CO}_2$  concentration does not show an accelerated post-1995 rise like the SSTs. Therefore other processes should contribute to this acceleration in SST-rise.

### **3.2 Regionally differentiated post-1995 SST accelerated-warming**

A pertinent question is whether the above observed accelerated rate of warming is spatially similar in the entire AS. In order to address this, we computed difference of the 60-month running-mean SST-trendline slopes between the post-1995 and the pre-1995 periods (Figure 2a). The result showed that the highest accelerated-warming is spatially-segregated and occurred along the north-eastern AS (off the Konkan, Saurashtra, Kutch and Makran coasts), off Oman, off northern-Somalia, central AS and parts of the southern AS. In order to study the temporal occurrence of the post-1995 accelerated-warming, the post-1995 SST slopes were computed for each month, but presented seasonally or sub-seasonally for brevity (Figures 2b-e). The seasons or sub-season presented were based on the monthly accelerated SST-rise. Accordingly, the average values for the months of January to February is designated as late-winter and the whole winter season, which includes the month of December, is not considered as the accelerated SST-rise was lesser. Other seasons include March to May as spring, June to September as summer (as this includes the period of the south-west monsoon) and October to November as fall. The highest accelerated-warming occurred seasonally in the late-winter in the north-eastern AS (see Figure 2b), in spring-season in the central and north-eastern AS (see Figure 2c), summer along the western-boundary of the AS (see Figure 2d) and in fall in the central AS (see Figure 2e). Having delineated the regions of highest accelerated-warming both

spatially and temporally, we now focus on the processes that are responsible for the observed changes.

### 3.3 Processes controlling the accelerated-warming

In order to decipher the factors leading to the observed spatial and temporal pattern of the highest accelerated-warming of SST, we have examined the slopes of the post-1995 wind, E-P (freshwater flux) and NHF, and their correlation coefficients with SST, all parameters being 5-year running-mean. To further understand which parameter dominantly-controlled the above-mentioned fluxes, we have analysed their components, but presented only the ones which significantly-influenced SST, besides the specific humidity. We present below the season-wise processes responsible for the highest accelerated-warming.

#### 3.3.1 Late-winter

The post-1995 accelerated-warming that occurred in the north-eastern AS during late-winter were significantly correlated with NHF and E-P at 95% confidence level (Figures 3a and 3c respectively). The slopes of the NHF (Figure 3b) showed an increasing-trend, while the E-P showed a decreasing-trend (Figure 3d). As could be inferred from Figure 3b the NHF increasing-trend into the ocean is due to the decreasing-trend of the LHF release to the atmosphere (Figure 3f). Similarly, an increasing-trend in the specific humidity (Figure 3j) leads to a decreasing-trend in the evaporation (Figure 3h) resulting in reduced-cooling. Thus, the combined-effect of both processes favoured an accelerated-warming. Recall that during winter the northern AS undergoes evaporative-cooling causing surface-densification. Subsequent convective-mixing leads to the mixed-layer deepening (Prasanna Kumar and Prasad, 1996; Wiggert *et al.*, 2000). The observed reducing-trend in post-1995 evaporation will thus lead to a lesser-cooling through the above-mentioned process in the north-eastern AS.

#### 3.3.2 Spring

During spring, the post-1995 accelerated-warming occurred in the north-eastern and central AS (Figure 2c). The central AS accelerated SST-rise was caused by the decreasing E-P trends (Figure 4b) and NHF increasing-trend into the ocean (Figure 4d), both of which occurred due to the decreasing-trends in evaporation (Figure 4f) and LHF (Figure 5a) release from the ocean to the atmosphere. Though the wind (Figure 5c) did not show any significant direct correlation with the spring-warming in the central AS, the wind-speed decreasing-trend (Figure 5d) in the central AS,

from March to May was responsible for the decreasing-trends of the evaporation and LHF release. Note that a small region of increasing specific humidity trend is also seen (Figure 5f), which can decrease evaporation leading to rise in SST. In the north-eastern AS the increasing-trend of NHF into the ocean, due to decreasing-trend of the LHF release to the atmosphere, occurred as a consequence of the specific humidity increasing-trend (Figure 5f). Significant negative correlation coefficients of SST with E-P (Figure 4a) and evaporation (Figure 4e) as well as positive correlation coefficients of SST with NHF (Figure 4c), LHF (Figure 5a) and specific humidity (Figure 5e) respectively, indicated the contributing factors that led to the accelerated warming in spring.

### 3.3.3 Summer-monsoon

The post-1995 accelerated SST-rise, in the summer-monsoon season (from June to September), occurred at two distinct regions along the western-boundary of the AS namely the Somali and the Arabian coasts. The averaged SST-difference, in the two periods, is shown using SODA SST data (Figure 6a). Along the Somalia coast the correlation coefficient between SST and wind-speed was significant at 95% level (Figure 7a), while off the Arabian coast the SST was significantly correlated with E-P at 95% level (Figure 7c). Note that along the Somali and Arabian coasts, the wind-speed showed a reducing-trend in the post-1995 period (Figure 7b). The intensity of reduction, however, was more along the Somali coast. The E-P, on the other hand, showed a reducing-trend only along the Arabian coast (Figure 7d). Here again, the mechanism that brought about the accelerated-warming in SST was different for both regions as would be shown below. An examination of the zonally-averaged (equator to 12°N) mean thermal structure during June to September in the upper 100m of the water column across the Somalia coast, derived from SODA, showed that the colder-isotherms during post-1995 surfaces closer to the coast than that during pre-1995 period (Figure 6b). For example, the 26°C isotherm surfaced at 51°E during post-1995 (red line), which was beyond 52°E during pre-1995 (black line). Similarly, in the vertical, the 25°C isotherm was at 15m depth during pre-1995 period, which was at 25m depth during post-1995, indicating the reduction in upwelling-intensity as well as its spatial-extent. This is also corroborated from the Figure 6a depicting the spatial pattern of June to September averaged pre and post-1995 SST. Thus, the above results demonstrated the role of ocean-dynamics in controlling the accelerated SST-warming in the Somali region. However, a similar analysis across the Arabian coast did not yield a similar result (figure not presented) indicating the role of processes other than reduced-upwelling contributing to the accelerated-warming too. Further analysis showed a significant correlation of evaporation with



SST at 95% level along the Arabian coast (Figure 7e) and the observed reducing-trend in evaporation during the post-1995 period (Figure 7f) was linked to the reducing-trend in the wind-speed implying the role of thermodynamic-processes controlling the accelerated SST-warming.

#### 3.3.4 Fall

The post-1995 accelerated SST-rise occurred in the months averaged from October to November in the central AS (Figure 2e). Correlation coefficients significant at 95% levels were seen between SST and NHF (Figure 8a) and also between SST and E-P (Figure 8c). The NHF into the ocean showed an increasing-trend (Figure 8b), while the E-P showed a decreasing-trend (Figure 8d).

The increasing-trend of the NHF into the ocean was due to a decreasing-trend LHF release from the ocean to the atmosphere (Figure 8f), which in turn was due to the increasing-trend in the specific humidity (Figure 9b). Besides the LHF, the reducing-trend in the release of LWR to the atmosphere (Figure 9d) also contributed to the increasing-trend of NHF into the ocean. The decreasing-trend of E-P was due to the reducing evaporation trend (Figure 9f). Thus, the increasing NHF trend into the ocean and decreasing-trend in the evaporation lead to higher SSTs.

#### **Summary and concluding remark**

We examined the regions, seasons and reasons for the post-1995 highest accelerated-warming seen in the AS using a suite of in-situ as well as remotely-sensed ocean and atmospheric data. The accelerated-warming did not occur uniformly throughout the AS. The regions of highest accelerated-warming were in the north-eastern AS during late-winter and spring, central AS in spring and fall and along the Somali and Arabian coasts during summer. In the north-eastern AS during late-winter, a post-1995 reduced-rate of evaporation resulted from an increasing-trend in the specific humidity, led to the accelerated-warming. However, the continued warming-trend exhibited by this region well into spring resulted from a reducing-trend in the LHF release to the atmosphere, due to an increasing-trend in the specific humidity. In the central AS, the accelerated-warming during spring was brought about by a combination of processes. A reducing-trend in the post-1995 winds caused reducing-trends in the evaporation and reducing-trends in the LHF release to the atmosphere, leading to an increasing NHF-trend into the ocean. In addition to this an increasing specific humidity trend in some parts in the central AS also leads to the same effect. During fall, an increasing-trend in the NHF into the ocean contributed by the decreasing-trends of the LHF and LWR release to the atmosphere lead to the accelerated-warming. Besides this, reducing-trends in evaporation in other part of the central AS also contributed to the accelerated post-1995 rise. In summer the reducing-

trend in the post-1995 winds caused a reduction in the upwelling-intensity as well as its spatial-extent along the Somali coast. In contrast, along the Arabian coast a reducing-trend in wind-speeds lead to lesser-evaporation, in-turn causing an accelerated-warming. Though North-East Arabian Sea shows an accelerated-warming in summer and fall too, the mechanisms that cause the warming in these seasons are not the same.

Some of the principal mechanisms by which the accelerated SST rise in the AS can occur are due to an increasing trend in the specific humidity causing a decrease in the evaporation and hence the decrease in E-P. Another mechanism is the increasing trend in the specific humidity causing a decreasing trend in the LHF release to the atmosphere, leading to a decreasing trend in the NHF release to the atmosphere, thus causing an increasing SST trend. Similarly, a decreasing wind speed can proceed a SST warming through reduced evaporation and E-P. The decreasing wind speeds can also reduce the upwelling off the Somali and Omani coasts in the summer causing a reduced cooling of SST. A reduction of the LWR release to the atmosphere can also cause a reduction in the NHF release to the atmosphere, thereby increasing the SST. The relative contributions of the heat, freshwater and momentum fluxes on the SST across-1995 are shown in table 2. The different air-sea processes and reduced upwelling along the Somali coast add to the rise caused by the increase in the carbon dioxide concentrations causing acceleration in the post-1995 SST rise in the Arabian Sea.

An increased rate of warming in the Arabian Sea, a region of very-high phytoplankton and fish production, can have serious implications to the structure and functioning of ecosystem. It can also impact the mid-depth oxygen minimum zone (OMZ) and seasonal-hypoxia experienced along the eastern boundary. A lot of future work has to be vested in understanding and quantifying the full-impact of accelerated-warming on ecosystem as it will alter the hydrological-cycle as well as food-web dynamics of this region.

### **Acknowledgements**

The authors thank Director CSIR-National Institute of Oceanography, Dona Paula, Goa and Council of Scientific and Industrial Research (CSIR), New Delhi for all the support and encouragement for this research. They also thank Mr. Shamkant Akerkar, Mr. Udayakumar Javali and Mrs. Sujal Bhandodkar for help with the figures. Joshua Rosario D'Mello would like to thank the CSIR for granting a fellowship and also the Principal and management of the Rosary College of Commerce and Arts, Navelim, Salcete, Goa. This is NIO contribution number xxxx.

### **Supporting Information**

Supporting information is available for the Arabian Sea basin-averaged number of ICOADS SST observations 60-month running-mean (Figure S1), the average number of ICOADS SST observations per month (Figure S2), the basin-averaged number of 60-month running-mean ICOADS SST and its envelope of standard error (Figure S3), and basin-averaged 60-month running means of ICOADS SST, NOAA Optimally Interpolated SST and Kaplan SSTA (Figure S4).

## References

- Alory G, Wijffels S, Meyers G. 2007. Observed temperature trends in the Indian Ocean over 1960–1999 and associated mechanisms. *Geophysical Research Letters* **34**: L02606. doi:[10.1029/2006GL028044](https://doi.org/10.1029/2006GL028044).
- Arrhenius S. 1896. On the influence of Carbonic Acid in the Air upon the Temperature of the Ground. *The London, Edinburgh, and Dublin Philosophical Magazine and Journal of Science. Series 5*, **41**: 237–276. doi: [10.1080/14786449608620846](https://doi.org/10.1080/14786449608620846).
- Bauer S, Hitchcock GL, Olson DB. 1991. Influence of monsoonally-forced Ekman dynamics upon the surface layer depth and plankton biomass distribution in the Arabian Sea. *Deep Sea Research Part I: Oceanographic Research Papers* **38**: 531–553. doi:[10.1016/0198-0149\(91\)90062-K](https://doi.org/10.1016/0198-0149(91)90062-K).
- Carton JA, Chepurin G, Cao X, Giese BS. 2000. A Simple Ocean Data Assimilation Analysis of the Global Upper Ocean 1950–95, Part I: Methodology. *Journal of Physical Oceanography* **30**: 294–309. doi:[http://dx.doi.org/10.1175/1520-0485\(2000\)030<0294:ASODAA>2.0.CO;2](http://dx.doi.org/10.1175/1520-0485(2000)030<0294:ASODAA>2.0.CO;2).
- Carton JA, Giese BS. 2008. A Reanalysis of Ocean Climate using Simple Ocean Data Assimilation (SODA). *Monthly Weather Review* **136**: 2999–3017. doi:<http://dx.doi.org/10.1175/2007MWR1978.1>.
- D’Mello JR, Prasanna Kumar S. 2015. Why is the Bay of Bengal experiencing a reduced rate of sea surface warming? *International Journal of Climatology*, **36**:1539–1548. doi:[10.1002/joc.4414](https://doi.org/10.1002/joc.4414).
- De Boyer Montégut C, Vilar J, Shenoi SSC, Shankar D, Durand F, Ethé C, Madec G. 2007. Simulated seasonal and interannual variability of the mixed layer budget in the northern Indian Ocean. *Journal of Climate* **20**: 3249–3268. doi:[10.1175/JCLI4148.1](https://doi.org/10.1175/JCLI4148.1).
- Dinesh Kumar PK, Steeven Paul Y, Muraleedharan KR, Murthy VSN, Preenu PR. 2016. Comparison of the long-term variability of Sea Surface Temperature in the Arabian Sea and Bay of Bengal. *Regional Studies in Marine Science* **3**: 67–75. doi:<http://dx.doi.org/10.1016/j.rsma.2015.05.004>.
- Findlater J. 1969. A major low-level air current near the Indian Ocean during the northern summer. *Quarterly Journal of the Royal Meteorological Society* **95**: 362–380. doi:[10.1002/qj.49709540409](https://doi.org/10.1002/qj.49709540409).
- Fischer, AS, Weller RA, Rudnick DL, Eriksen CC, Lee CM, Brink KH, Fox CA, Leben RR. 2002. Mesoscale eddies, coastal upwelling, and the upper-ocean heat budget in the Arabian Sea. *Deep-Sea Research Part II-Topical Studies in Oceanography* **49**: 2231–2264. doi:[10.1016/s0967-0645\(02\)00036-x](https://doi.org/10.1016/s0967-0645(02)00036-x).

- Foukal P, Fröhlich C, Spruit H, Wigley TML. 2006. Variations in solar luminosity and their effect on the Earth's climate. *Nature* **443**: 161–1666. doi:[10.1038/nature05072](https://doi.org/10.1038/nature05072).
- Gulev S, T Jung, Ruprecht E. 2007. Estimation of the Impact of Sampling Errors in the VOS Observations on Air–Sea Fluxes. Part I: Uncertainties in Climate Means. *Journal of Climate* **20**: 279–301. doi:[10.1175/JCLI4010.1](https://doi.org/10.1175/JCLI4010.1).
- Gulev S, T Jung, Ruprecht E. 2007. Estimation of the Impact of Sampling Errors in the VOS Observations on Air–Sea Fluxes. Part II: Impact on Trends and Interannual Variability. *Journal of Climate* **20**: 302–315. doi:[10.1175/JCLI4008.1](https://doi.org/10.1175/JCLI4008.1).
- Haigh JD, Winning AR, Toumi R, Harder JW. 2010. An influence of solar spectral variations on radiative forcing of climate. *Nature* **467**: 696–699. doi:[10.1038/nature09426](https://doi.org/10.1038/nature09426).
- Han W, Vialard J, McPhaden MJ, Lee T, Masumoto Y, Feng M, de Ruijter WPM. 2014. Indian Ocean Decadal Variability: A Review. *Bulletin of the American Meteorological Society* **95**: 1679–1703. doi:<http://dx.doi.org/10.1175/BAMS-D-13-00028.1>.
- Josey SA. 2001. A comparison of ECMWF, NCEP-NCAR, and SOC surface heat fluxes with moored buoy measurements in the subduction region of the northeast Atlantic. *Journal of Climate* **14**: 1780–1789. doi:[http://dx.doi.org/10.1175/1520-0442\(2001\)014<1780:ACOENN>2.0.CO;2](http://dx.doi.org/10.1175/1520-0442(2001)014<1780:ACOENN>2.0.CO;2).
- Kalnay E, Kanamitsu M, Kistler R, Collins W, Deaven D, Gandin L, Iredell M, Saha S, White G, Woollen J, Zhu Y, Leetmaa A, Reynolds R, Chelliah M, Ebisuzaki W, Higgins W, Janowiak J, Mo KC, Ropelewski C, Wang J, Jenne R, Joseph D. 1996. The NCEP/NCAR 40-year reanalysis project. *Bulletin of the American Meteorological Society* **77**: 437–470. doi:[http://dx.doi.org/10.1175/1520-0477\(1996\)077<0437:TNYRP>2.0.CO;2](http://dx.doi.org/10.1175/1520-0477(1996)077<0437:TNYRP>2.0.CO;2).
- Keeling CD, Piper SC, Bacastow RB, Wahlen M, Whorf TP, Heimann M, Meijer HA. 2001. Exchanges of atmospheric CO<sub>2</sub> and <sup>13</sup>CO<sub>2</sub> with the terrestrial biosphere and oceans from 1978 to 2000. I. Global aspects, SIO Reference Series, No. 01-06, Scripps Institution of Oceanography, San Diego, 88 pages.
- Keeling CD, Piper SC, Bacastow RB, Wahlen M, Whorf TP, Heimann M, Meijer HA. 2005. Atmospheric CO<sub>2</sub> and <sup>13</sup>CO<sub>2</sub> exchange with the terrestrial biosphere and oceans from 1978 to 2000: observations and carbon cycle implications, pages 83-113, in *A History of Atmospheric CO<sub>2</sub> and its effects on Plants, Animals, and Ecosystems*, edited by Ehleringer JR, TE Cerling, MD Dearing, pp. 83-133, Springer Verlag, New York.
- Kennedy JJ, Rayner NA, Smith RO, Saunby M, Parker DE. 2011a. Reassessing biases and other uncertainties in sea-surface temperature observations since 1850 part 1: measurement and sampling errors. *Journal of Geophysical Research* **116**: D14103. doi:[10.1029/2010JD015218](https://doi.org/10.1029/2010JD015218).
- Kennedy JJ, Rayner NA, Smith RO, Saunby M, Parker DE. 2011b. Reassessing biases and other uncertainties in sea-surface temperature observations since 1850 part 2: biases and homogenisation. *Journal of Geophysical Research* **116**: D14104. doi:[10.1029/2010JD015220](https://doi.org/10.1029/2010JD015220).

- Kubota M, Iwabe N, Cronin MF, Tomita H. 2008. Surface heat fluxes from the NCEP/NCAR and NCEP/DOE reanalyses at the Kuroshio Extension Observatory buoy site. *Journal of Geophysical Research* **113**: C02009. doi:[10.1029/2007JC004338](https://doi.org/10.1029/2007JC004338).
- McCreary Jr., JP, Kohler KE, Hood RR, Smith S, Kindle J, Fischer A, Weller RA. 2001. Influences of diurnal and intraseasonal forcing on mixed-layer and biological variability in the central Arabian Sea. *Journal of Geophysical Research* **106(C4)**: 7139–7155. doi:[10.1029/2000JC900156](https://doi.org/10.1029/2000JC900156).
- Moore GWK, Renfrew IA. 2002. An assessment of the surface turbulent heat fluxes from the NCEP-NCAR reanalysis over the western boundary currents. *Journal of Climate* **15**: 2020–2037. doi:[http://dx.doi.org/10.1175/1520-0442\(2002\)015<2020:AAOTST>2.0.CO;2](http://dx.doi.org/10.1175/1520-0442(2002)015<2020:AAOTST>2.0.CO;2).
- Prasanna Kumar S, Prasad TG. 1996. Winter cooling in the Northern Arabian Sea. *Current Science* **71**: 834–841.
- Prasanna Kumar S, Madhupratap M, Dileep Kumar M, Muraleedharan PM, de Sousa SN, Sawant S, Gauns M, Sarma VVSS. 2001. High biological productivity in the central Arabian Sea during the summer monsoon driven by Ekman pumping and lateral advection. *Current Science* **81**: 1633–1638.
- Prasanna Kumar S, Roshin RP, Narvekar J, Dinesh Kumar PK, Vivekanandan E. 2009. Response of the Arabian Sea to global warming and associated regional climate shift. *Marine Environmental Research* **68**: 217–222, doi:[10.1016/j.marenvres.2009.06.010](https://doi.org/10.1016/j.marenvres.2009.06.010).
- Ramesh Babu V, Sastry JS. 1984. Summer cooling in the east central Arabian Sea: A process of dynamic response to the southwest monsoon. *Mausam* **35**: 17–26.
- Rayner NA, Parker DE, Horton EB, Folland CK, Alexander LV, Rowell DP, Kent EC and Kaplan A. 2003. Global analyses of sea surface temperature, sea ice, and night marine air temperature since the late nineteenth century. *Journal of Geophysical Research* **108**: (D14), 4407. doi:[10.1029/2002JD002670](https://doi.org/10.1029/2002JD002670).
- Rayner NA, Brohan P, Parker DE, Folland CK, Kennedy JJ, Vanicek M, Ansell TJ, Tett SFB. 2006. Improved Analyses of Changes and Uncertainties in Sea Surface Temperature Measured In Situ Since Mid-Nineteenth Century: The HadSST2 Dataset. *Journal of Climate* **19**: 446–469. doi:<http://dx.doi.org/10.1175/JCLI3637.1>
- Roxy MK, Ritika K, Terray P, Masson S. 2014. The Curious Case of Indian Ocean Warming. *Journal of Climate* **27**: 8501–8509. doi:<http://dx.doi.org/10.1175/JCLI-D-14-00471.1>.
- Rupa Kumar S, Krishna Kumar K, Ashrit RG, Patwardhan SK, Pant GB. 2002. Climate Change in India- Observations and Model Projections: Climate Change and India- Issues Concerns and Oppurtunities, Ed. P. R. Shukla, S. K. Sharma, and P. V. Ramana, pages 24–75, Tata McGraw-Hill Publishing Company Limited, New Delhi.
- Schwabe H, H Schwabe Herrn. 1844. Sonnen-Beobachtungen im Jahre 1843. *Astronomische Nachrichten* **21**: 234–235. doi: [10.1002/asna.18440211505](https://doi.org/10.1002/asna.18440211505).
- Sharma GS. 1966. Thermocline as an indicator of upwelling. *Journal of the Marine Biological Association of India* **8**: 8–19.

- Smith RL, Bottero JS. 1977. *On Upwelling in the Arabian Sea: A Voyage of Discovery*, Pergamon Press, New York.
- Smith SL, Codispoti LA. 1980. Southwest monsoon of 1979: chemical and biological response of Somali coastal waters. *Science* **209**: 597–600. doi:[10.1126/science.209.4456.597](https://doi.org/10.1126/science.209.4456.597).
- Smith SR, Legler DM, Verzone KV. 2001. Quantifying Uncertainties in NCEP Reanalyses Using High-Quality Research Vessel Observations. *Journal of Climate* **14**: 4062–4072. doi:[http://dx.doi.org/10.1175/1520-0442\(2001\)014<4062:QUINRU>2.0.CO;2](http://dx.doi.org/10.1175/1520-0442(2001)014<4062:QUINRU>2.0.CO;2)
- Varadachari VVR, Sharma GS. 1967. Circulation of the surface waters in the North Indian Ocean. *The Journal of Indian Geophysical Union* **4**: 61–73.
- Weller RA, Fischer AS, Rudnick DL, Eriksen CC, Dickey TD, Marra J, Fox C, Leben R. 2002. Moored observations of upper-ocean response to the monsoons in the Arabian Sea in 1994–1995. *Deep-Sea Research II* **49**: 2195–2230. doi:[10.1016/S0967-0645\(02\)00035-8](https://doi.org/10.1016/S0967-0645(02)00035-8).
- Willson RC, Hudson HS. 1991. The Sun's luminosity over a complete solar cycle. *Nature* **351**: 42–44. doi:[10.1038/351042a0](https://doi.org/10.1038/351042a0).
- Wiggert JD, Jones BH, Dickey TD, Brink KH, Weller RA, Marra J, Codispoti LA. 2000. The Northeast Monsoons's impact on mixing, phytoplankton biomass and nutrient cycling in the Arabian Sea. *Deep-Sea Research Part II: Topical Studies in Oceanography* **47**: 1353–1385. doi:[10.1016/S0967-0645\(99\)00147-2](https://doi.org/10.1016/S0967-0645(99)00147-2).
- White WB, Lean J, Cayan DR, Dettinger MD. 1997. Response of global upper ocean temperature to changing solar irradiance. *Journal of Geophysical Research* **102**: 3255–3266. doi:[10.1029/96JC03549](https://doi.org/10.1029/96JC03549).
- Woodruff SD, Worley SJ, Lubker SJ, Ji Z, Freeman JE, Berry DI, Brohan P, Kent EC, Reynolds RW, Smith SR, Wilkinson C. 2011. ICOADS Release 2.5: Extensions and enhancements to the surface marine meteorological archive. *International Journal of Climatology (CLIMAR-III Special Issue)* **31**: 951–967. doi:[10.1002/joc.2103](https://doi.org/10.1002/joc.2103).
- Yu L, Jin X, Weller RA. 2008. Multidecade Global Flux Datasets from the Objectively Analyzed Air-sea Fluxes (OAFlux) Project: Latent and sensible heat fluxes, ocean evaporation, and related surface meteorological variables. Woods Hole Oceanographic Institution, OAFlux Project Technical Report. OA-2008-01, 64pp. Woods Hole, Massachusetts.

## Figure Captions

**Figure 1.** Arabian Sea (Eq.- 25 °N, 45 °E- 80 °E) SST 60-month running-mean (thick black line) from 1960 January to 2011 December, with trendlines for the entire period (thin black line) and in the pre and post 1995 November periods (thin black dashed lines), Sunspot Number 60-month running-mean (thin blue line) and Carbon dioxide Concentration 60-month running-mean (thin red line with cross marks).

**Figure 2.** Arabian Sea slope difference (°C/year) between the periods from 1995 November to 2011 December and 1960 January to 1995 November, of SST 60-month running-mean (Fig. 2a) and of SST 5-year running-means in late-winter (January to February) (Fig. 2b), spring season (March to May) (Fig. 2c), summer (June to September) (Fig. 2d) and fall season (October to November) (Fig. 2e). The regions are shaded (dotted) if significant at the 95 % level. The regions are shaded above and contoured at  $|t\text{-value}| > 1.964$ , number of points (N) = 560 (Fig. 2a);  $|t\text{-value}| > 2.015$ , N = 44 (Figs. 2b-2d) and  $|t\text{-value}| > 2.014$ , N= 45 (Fig. 2e). The approximate region of highest accelerated SST warming is indicated by a dashed ellipse or circle.

**Figure 3.** Arabian Sea late-winter season (January to February) averaged, correlation coefficients of SST with net heat flux (NHF) (3a), evaporation precipitation difference (E-P) (3c), latent heat flux (LHF) (3e), evaporation (3g) and specific humidity (3i), coloured for regions having 95 % and above significance level ( $r > |±0.5325|$ , N=14). Late-winter season averaged slopes of NHF ((W/m<sup>2</sup>)/year) (3b), E-P ((cm/year)/year) (3d), LHF ((W/m<sup>2</sup>)/year) (3f), evaporation ((cm/year)/year) (3h) and specific humidity ((g/kg)/year) (3j), are shaded for regions having 95 % and above significance level (2-tailed t-statistic GE  $|±2.18|$ , N=14). Both NHF and LHF are considered positive into the ocean. The approximate region of highest accelerated SST warming is indicated by a dashed ellipse.

**Figure 4.** Arabian Sea spring season (March to May) averaged, correlation coefficients of SST with evaporation precipitation difference (E-P) (4a), net heat flux (NHF) (4c) and evaporation (4e), coloured for regions having 95 % and above significance level ( $r > |±0.5325|$ , N=14). Spring season averaged slopes of E-P ((cm/year)/year) (4b), NHF ((W/m<sup>2</sup>)/year) (4d) and evaporation ((cm/year)/year) (4f), are shaded (cross-hatching) for regions having 95 % and above significance level (2-tailed t-statistic GE  $|±2.18|$ , N=14). NHF is considered positive into the ocean. The approximate regions of highest accelerated SST warming are indicated by a dashed ellipse or circle.

**Figure 5.** Arabian Sea spring season (March to May) averaged, correlation coefficients of SST with latent heat flux (LHF) (5a), wind speed (5c) and specific humidity (5e), coloured for regions having 95 % and above significance level ( $r > |±0.5325|$ , N=14). Spring season averaged slopes of LHF ((W/m<sup>2</sup>)/year) (5b), wind speed ((m/s)/year) (5d) and specific humidity ((g/kg)/year) (5f), are shaded (cross-hatching) for regions having 95 % and above significance level (2-tailed t-statistic GE  $|±2.18|$ , N=14). LHF is considered positive into the ocean. The approximate regions of highest accelerated SST warming are indicated by a dashed ellipse or circle.

**Figure 6.** Arabian Sea averaged June to September, Simple Ocean Data Assimilation (SODA): a) Surface temperature (°C), at 5 m depth, shaded in the period averaged from 1960 January to 2011 December, contoured in the period from 1960 January to 1995 November (black) and from 1995 November to 2011 December (red); and b) temperature (°C) section till 100 m depth, averaged off the Somali coast (Eq. to 12 °N) in the period from 1960 January to 1995 November (black) and 1995 November to 2011 December (red).

**Figure 7.** Arabian Sea summer season (June to September) averaged, correlation coefficients of SST with wind speed (7a), evaporation precipitation difference (E-P) (7c) and evaporation (7e), coloured for regions having 95 % and above significance level ( $r > |±0.5325|$ , N=14). Summer season averaged slopes of wind speed ((m/s)/year) (7b), E-P ((cm/year)/year) (7d) and evaporation ((cm/year)/year) (7f) are shaded (cross-hatching) for regions having 95 % and above significance level (2-tailed t-statistic GE  $|±2.18|$ , N=14). The approximate regions of highest accelerated SST warming are indicated by dashed ellipses.

**Figure 8.** Arabian Sea fall season (October to November) averaged, correlation coefficients of SST with net heat flux (NHF) (8a), evaporation precipitation difference (E-P) (8c) and latent heat flux (LHF) (8e), coloured for regions having 95% and above significance level ( $r > |±0.514|$ , N=15). Spring season averaged slopes of NHF ((W/m<sup>2</sup>)/year) (8b), E-P ((cm/year)/year) (8d) and LHF ((W/m<sup>2</sup>)/year) (8f), are shaded (cross-hatching) for regions having 95 % and above significance level (2-tailed t-statistic GE  $|±2.160|$ , N=15). NHF and LHF are considered positive into the ocean. The approximate region of highest accelerated SST warming is indicated by a dashed circle.

**Figure 9.** Arabian Sea fall season (October to November) averaged, correlation coefficients of SST with specific humidity (9a), longwave radiation (LWR) (9c) and evaporation (9e), coloured for regions having 95% and above significance level ( $r > |±0.514|$ , N=15). Spring season averaged slopes of specific humidity ((g/kg)/year) (9b), LWR ((W/m<sup>2</sup>)/year) (9d) and evaporation ((cm/year)/year) (9f), are shaded (cross-hatching) for regions having 95 % and above significance level (2-tailed t-statistic GE  $|±2.160|$ , N=15). LWR is considered positive into the ocean. The approximate region of highest accelerated SST warming is indicated by a dashed circle.



**Table 1.** Sources of data and their specifications.

Name of the Dataset	Parameters	Period	Temporal and Spatial Interval	URL	References/ Source
International Comprehensive Ocean-Atmosphere Data Set (ICOADS)	Sea Surface Temperature (SST), Specific Humidity, Wind components	1960-2011	Monthly; $1^{\circ} \times 1^{\circ}$	<a href="http://www.esrl.noaa.gov/psd/data/gridded/data.coads.1deg.html">www.esrl.noaa.gov/psd/data/gridded/data.coads.1deg.html</a>	Woodruff <i>et al.</i> , 2011
Objectively Analyzed Air-Sea Fluxes (OAFflux)	Evaporation rate	1960-2011	Monthly; $1^{\circ} \times 1^{\circ}$	Now available at <a href="http://rda.ucar.edu/datasets/ds260.1/">http://rda.ucar.edu/datasets/ds260.1/</a>	Yu <i>et al.</i> , 2008
CDC Derived NCEP Reanalysis Products Surface Flux	Precipitation	1960-2011	Monthly; $\sim 1.875^{\circ} \times 1.875^{\circ}$	<a href="ftp://ftp.cdc.noaa.gov/DataSets/ncep.reanalysis.derived/surface_gauss/prate.sfc.mon.mean.nc">ftp://ftp.cdc.noaa.gov/DataSets/ncep.reanalysis.derived/surface_gauss/prate.sfc.mon.mean.nc</a>	Kalnay <i>et al.</i> , 1996
NCEP/NCAR reanalysis monthly means and other derived variables data	Shortwave radiation (SWR), Longwave radiation (LWR), Latent Heat Flux (LHF) and Sensible Heat Flux (SHF)	1960-2011	Monthly; T62 Gaussian grid ( $192 \times 94$ )	<a href="http://www.esrl.noaa.gov/psd/data/gridded/data.ncep.reanalysis.derived.surfaceflux.html">http://www.esrl.noaa.gov/psd/data/gridded/data.ncep.reanalysis.derived.surfaceflux.html</a>	Kalnay <i>et al.</i> , 1996
WDC-SILSO, Royal Observatory of Belgium, Brussels Sunspot Number data	International sunspot number	1960-2011	Monthly; Global	Now available at <a href="http://www.sidc.be/silso/datafiles">www.sidc.be/silso/datafiles</a>	WDC-SILSO, Royal Observatory of Belgium, Brussels
Keeling Carbon Dioxide Concentration Data	Carbon dioxide atmospheric concentration	1960-2011	Monthly; Mauna Loa (1960 January- 1979 December); Global (1980 January- 2011 December)	<a href="ftp://ftp.cmdl.noaa.gov/ccg/co2/trends/co2_mm_mlo.txt">ftp://ftp.cmdl.noaa.gov/ccg/co2/trends/co2_mm_mlo.txt</a> (Mauna Loa); <a href="ftp://ftp.cmdl.noaa.gov/ccg/co2/trends/co2_mm_gl.txt">ftp://ftp.cmdl.noaa.gov/ccg/co2/trends/co2_mm_gl.txt</a> (Global)	Keeling <i>et al.</i> , 2001; Keeling <i>et al.</i> , 2005
Simple Ocean Data Assimilation (SODA) data v2.2.4	Temperature Section	1960-2010	Monthly; $0.5^{\circ} \times 0.5^{\circ}$ ; 40 vertical levels	<a href="http://apdr.csoest.hawaii.edu/las/v6/constrain?var=3076">http://apdr.csoest.hawaii.edu/las/v6/constrain?var=3076</a>	Carton <i>et al.</i> , 2000; Carton and Giese, 2008

**Table 2.** Variance between 60-month running-means of the SST and the various fluxes, in the Arabian Sea.

	<b>Net Heat Flux</b>	<b>Evaporation Precipitation Difference</b>	<b>Wind Speed</b>
1962 July to 1995 November	0.05	0.28	0.35
1995 November to 2009 June	0.34	0.13	0.51

## Figures

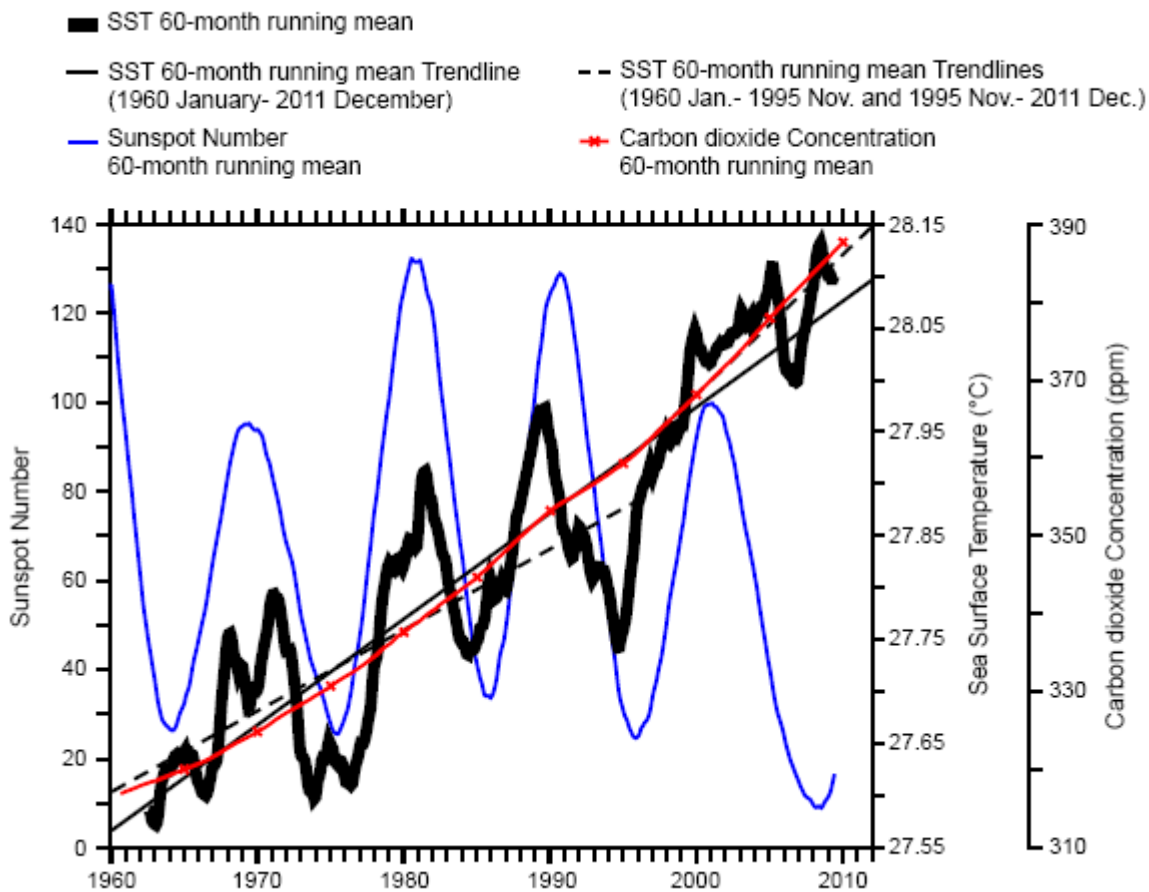


**Figure 1.** Arabian Sea (Eq.- 25 °N, 45 °E- 80 °E) SST 60-month running-mean (thick black line) from 1960 January to 2011 December, with trendlines for the entire period (thin black line) and in the pre and post 1995 November periods (thin black dashed lines), Sunspot Number 60-month running-mean (thin blue line) and Carbon dioxide Concentration 60-month running-mean (thin red line with cross marks).

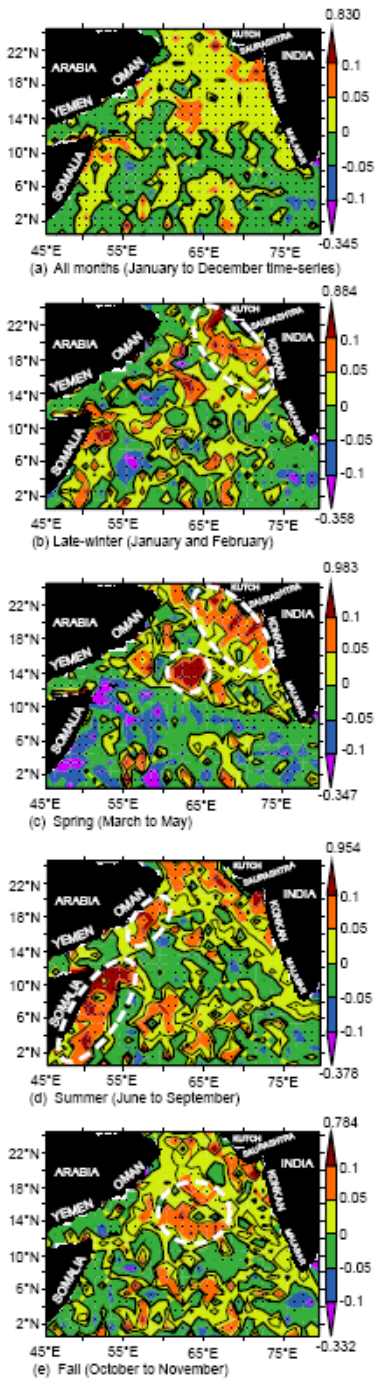


**Figure 2.** Arabian Sea slope difference ( $^{\circ}\text{C}/\text{year}$ ) between the periods from 1995 November to 2011 December and 1960 January to 1995 November, of SST 60-month running-mean (Fig. 2a) and of SST 5-year running-means in late-winter (January to February) (Fig. 2b), spring season (March to May) (Fig. 2c), summer (June to September) (Fig. 2d) and fall season (October to November) (Fig. 2e). The regions are shaded (dotted) if significant at the 95 % level. The regions are shaded above and contoured at  $|t\text{-value}| > 1.964$ , number of points ( $N$ ) = 560 (Fig. 2a);  $|t\text{-value}| > 2.015$ ,  $N = 44$  (Figs. 2b-2d) and  $|t\text{-value}| > 2.014$ ,  $N = 45$  (Fig. 2e). The approximate region of highest accelerated SST warming is indicated by a dashed ellipse or circle.

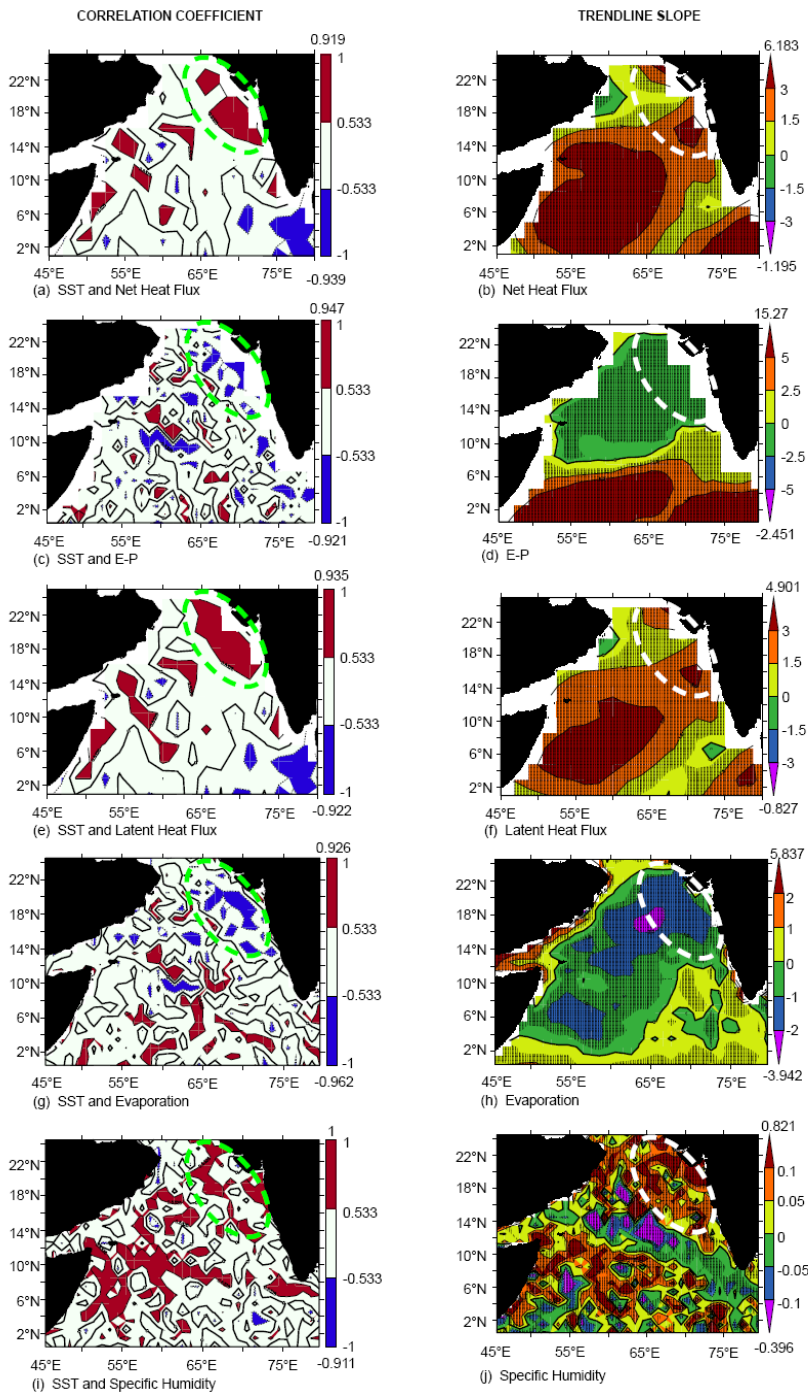


**Figure 3.** Arabian Sea late-winter season (January to February) averaged, correlation coefficients of SST with net heat flux (NHF) (3a), evaporation precipitation difference (E-P) (3c), latent heat flux (LHF) (3e), evaporation (3g) and specific humidity (3i), coloured for regions having 95 % and above significance level ( $r > | \pm 0.5325 |$ ,  $N=14$ ). Late-winter season averaged slopes of NHF ( $(W/m^2)/year$ ) (3b), E-P ( $(cm/year)/year$ ) (3d), LHF ( $(W/m^2)/year$ ) (3f), evaporation ( $(cm/year)/year$ ) (3h) and specific humidity ( $(g/kg)/year$ ) (3j), are shaded for regions having 95 % and above significance level (2-tailed t-statistic  $GE | \pm 2.18 |$ ,  $N=14$ ). Both NHF and LHF are considered positive into the ocean. The approximate region of highest accelerated SST warming is indicated by a dashed ellipse.

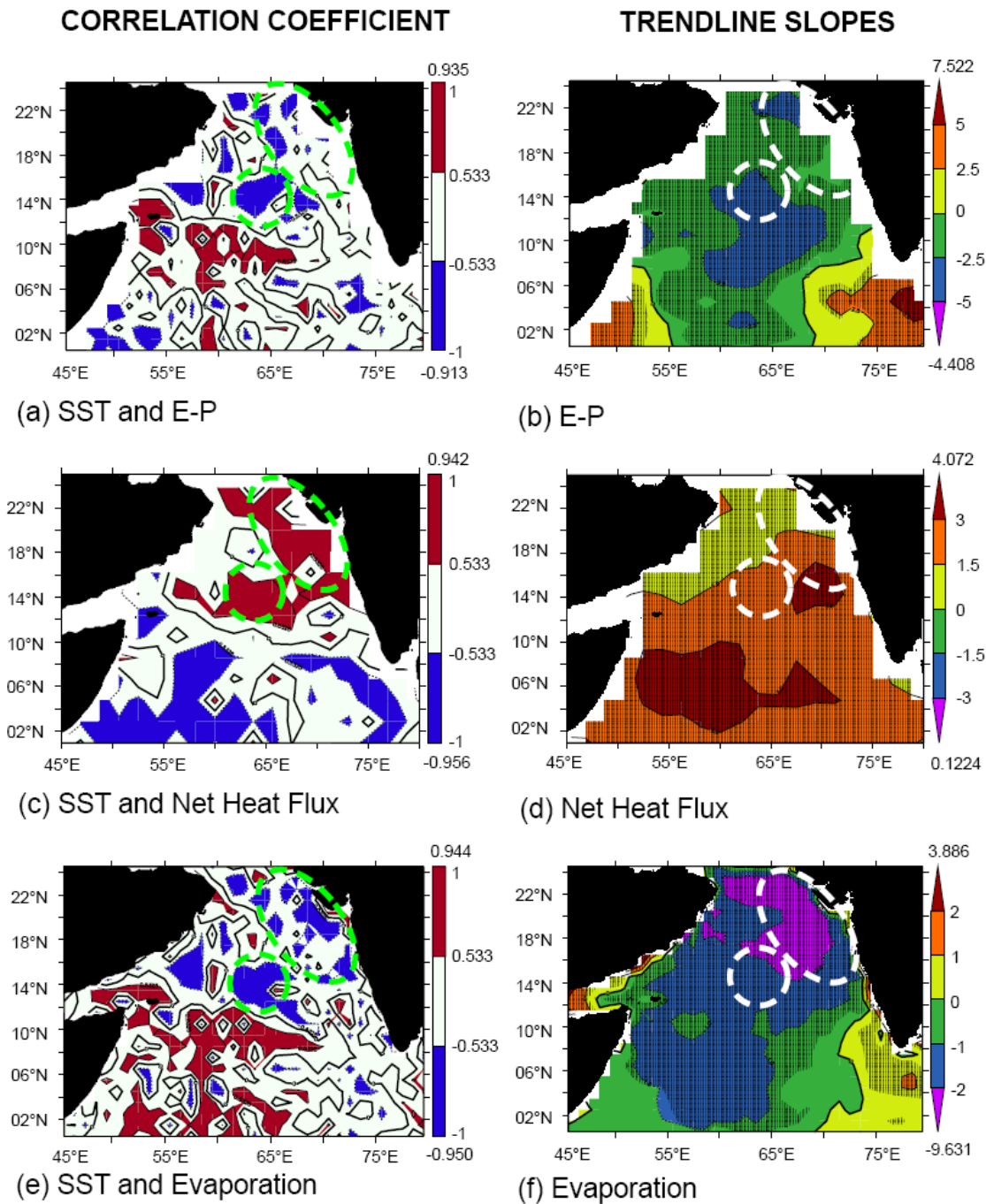


**Figure 4.** Arabian Sea spring season (March to May) averaged, correlation coefficients of SST with evaporation precipitation difference (E-P) (4a), net heat flux (NHF) (4c) and evaporation (4e), coloured for regions having 95 % and above significance level ( $r > |±0.5325|$ ,  $N=14$ ). Spring season averaged slopes of E-P ((cm/year)/year) (4b), NHF ((W/m<sup>2</sup>)/year) (4d) and evaporation ((cm/year)/year) (4f), are shaded (cross-hatching) for regions having 95 % and above significance level (2-tailed t-statistic GE  $|±2.18|$ ,  $N=14$ ). NHF is considered positive into the ocean. The approximate regions of highest accelerated SST warming are indicated by a dashed ellipse or circle.

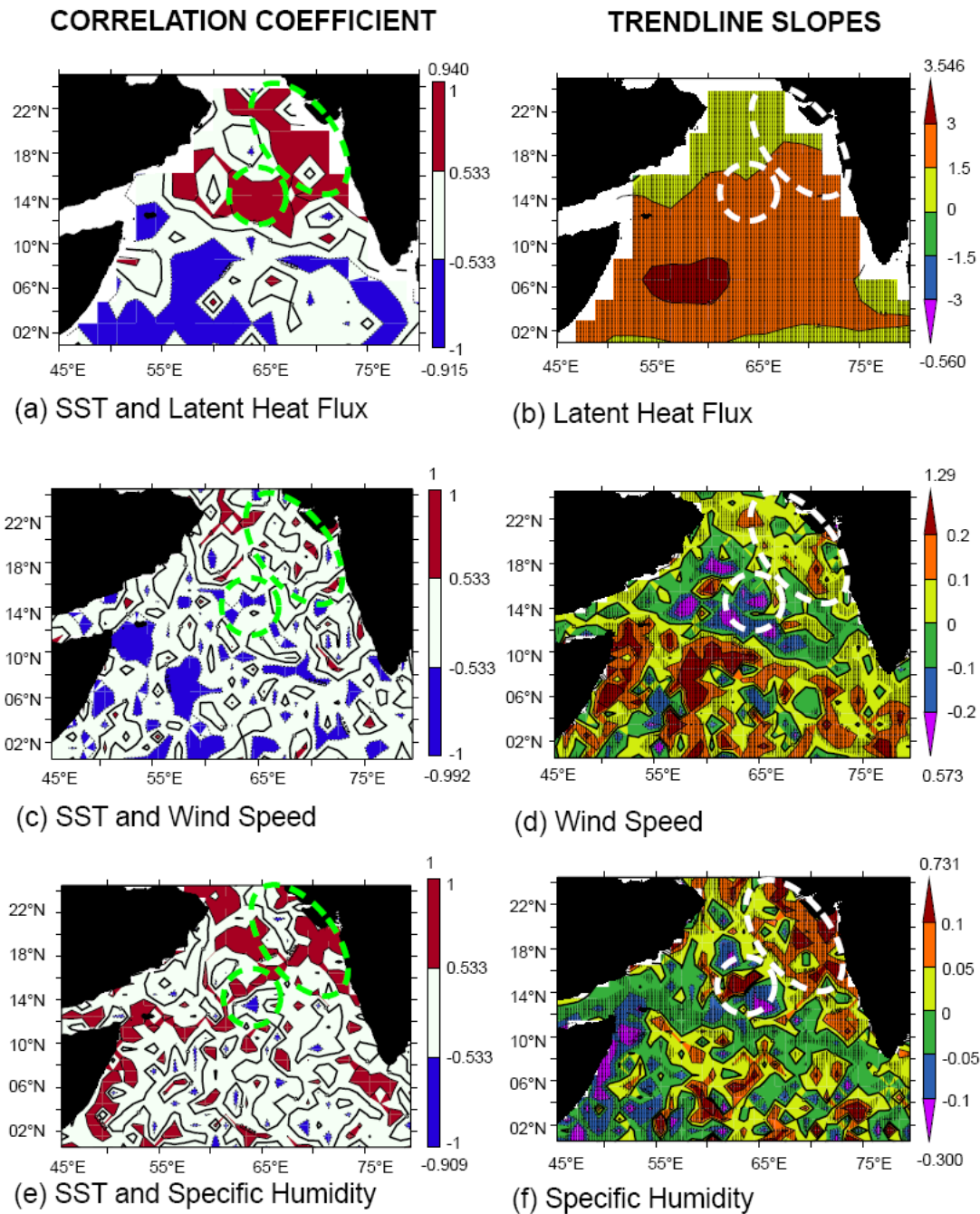


**Figure 5.** Arabian Sea spring season (March to May) averaged, correlation coefficients of SST with latent heat flux (LHF) (5a), wind speed (5c) and specific humidity (5e), coloured for regions having 95 % and above significance level ( $r > | \pm 0.5325 |$ ,  $N=14$ ). Spring season averaged slopes of LHF ( $(W/m^2)/year$ ) (5b), wind speed ( $(m/s)/year$ ) (5d) and specific humidity ( $(g/kg)/year$ ) (5f), are shaded (cross-hatching) for regions having 95 % and above significance level (2-tailed t-statistic  $GE | \pm 2.18 |$ ,  $N=14$ ). LHF is considered positive into the ocean. The approximate regions of highest accelerated SST warming are indicated by a dashed ellipse or circle.

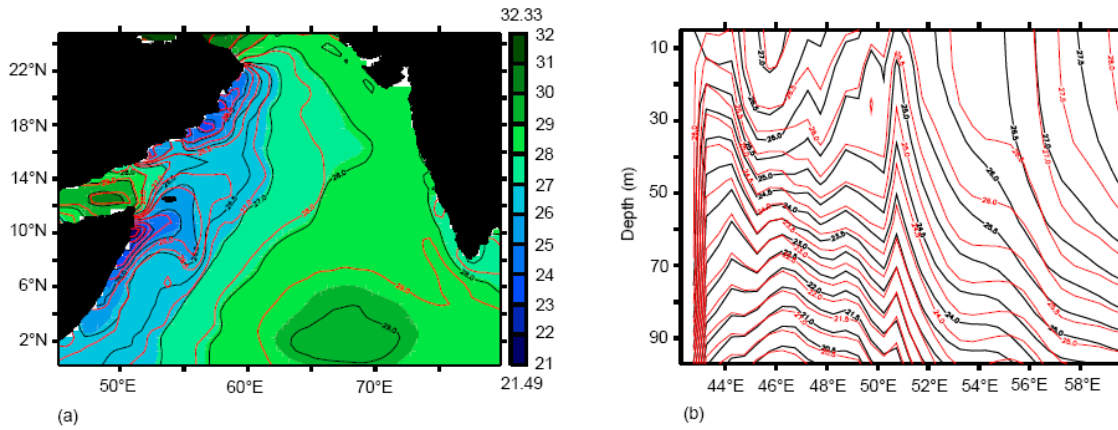


**Figure 6.** Arabian Sea averaged June to September, Simple Ocean Data Assimilation (SODA): a) Surface temperature ( $^{\circ}\text{C}$ ), at 5 m depth, shaded in the period averaged from 1960 January to 2011 December, contoured in the period from 1960 January to 1995 November (black) and from 1995 November to 2011 December (red); and b) temperature ( $^{\circ}\text{C}$ ) section till 100 m depth, averaged off the Somali coast (Eq. to  $12^{\circ}\text{N}$ ) in the period from 1960 January to 1995 November (black) and 1995 November to 2011 December (red).



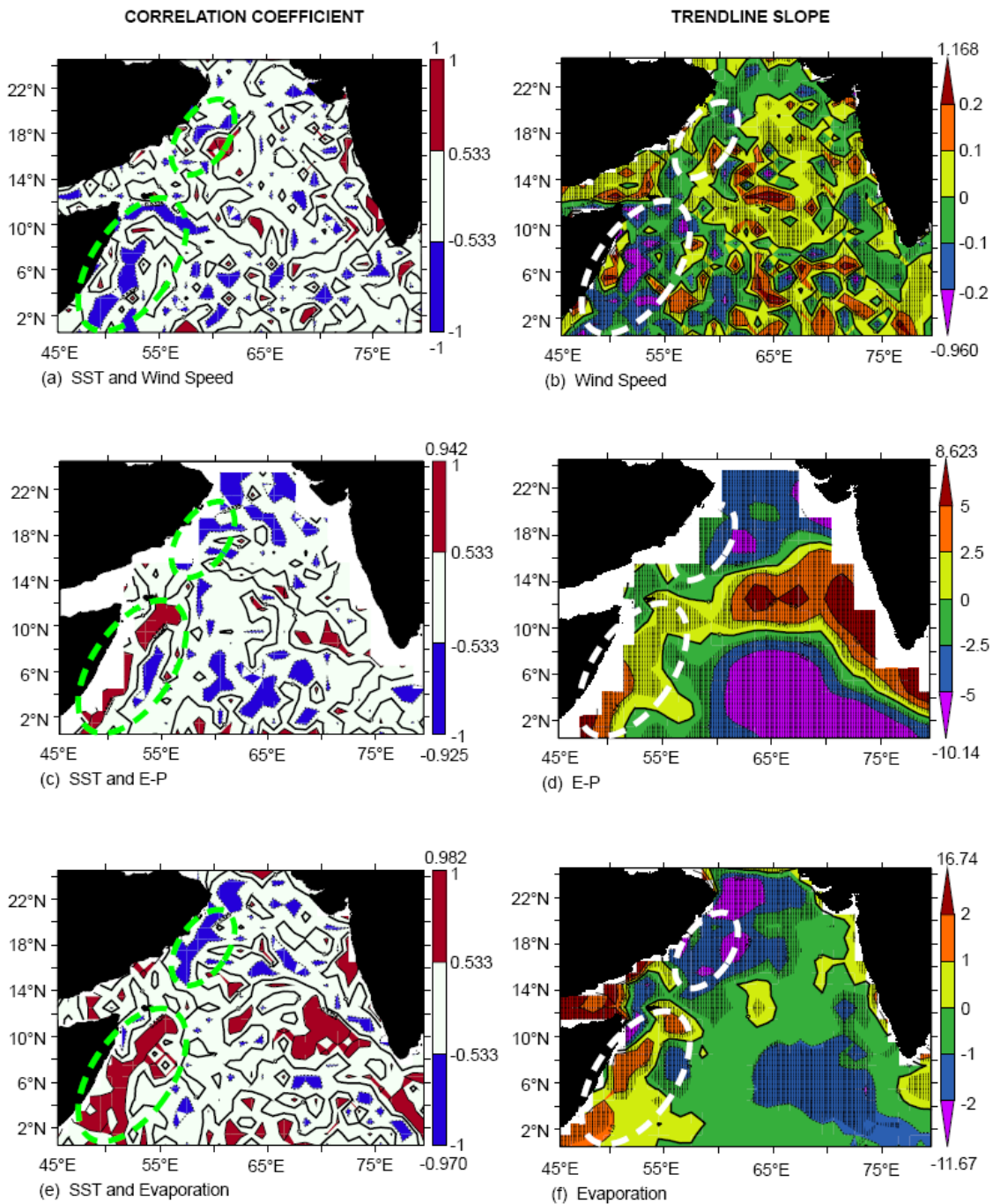


**Figure 7.** Arabian Sea summer season (June to September) averaged, correlation coefficients of SST with wind speed (7a), evaporation precipitation difference (E-P) (7c) and evaporation (7e), coloured for regions having 95 % and above significance level ( $r > |±0.5325|$ ,  $N=14$ ). Summer season averaged slopes of wind speed ((m/s)/year) (7b), E-P ((cm/year)/year) (7d) and evaporation ((cm/year)/year) (7f) are shaded (cross-hatching) for regions having 95 % and above significance level (2-tailed t-statistic  $GE > |±2.18|$ ,  $N=14$ ). The approximate regions of highest accelerated SST warming are indicated by dashed ellipses.

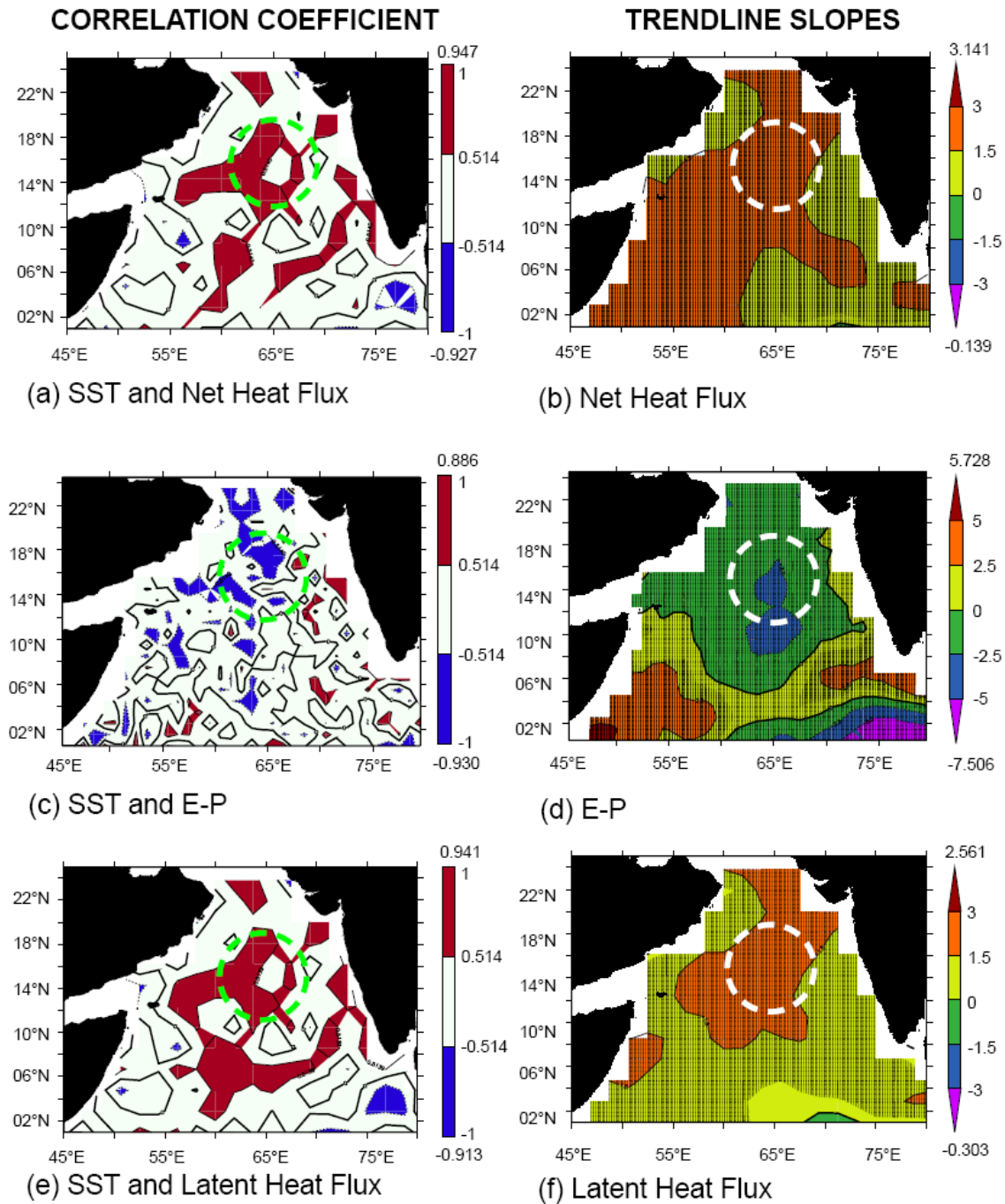


**Figure 8.** Arabian Sea fall season (October to November) averaged, correlation coefficients of SST with net heat flux (NHF) (8a), evaporation precipitation difference (E-P) (8c) and latent heat flux (LHF) (8e), coloured for regions having 95% and above significance level ( $r > |±0.514|$ ,  $N=15$ ). Spring season averaged slopes of NHF ( $(W/m^2)/year$ ) (8b), E-P ( $(cm/year)/year$ ) (8d) and LHF ( $(W/m^2)/year$ ) (8f), are shaded (cross-hatching) for regions having 95 % and above significance level (2-tailed t-statistic  $GE |±2.160|$ ,  $N=15$ ). NHF and LHF are considered positive into the ocean. The approximate region of highest accelerated SST warming is indicated by a dashed circle.

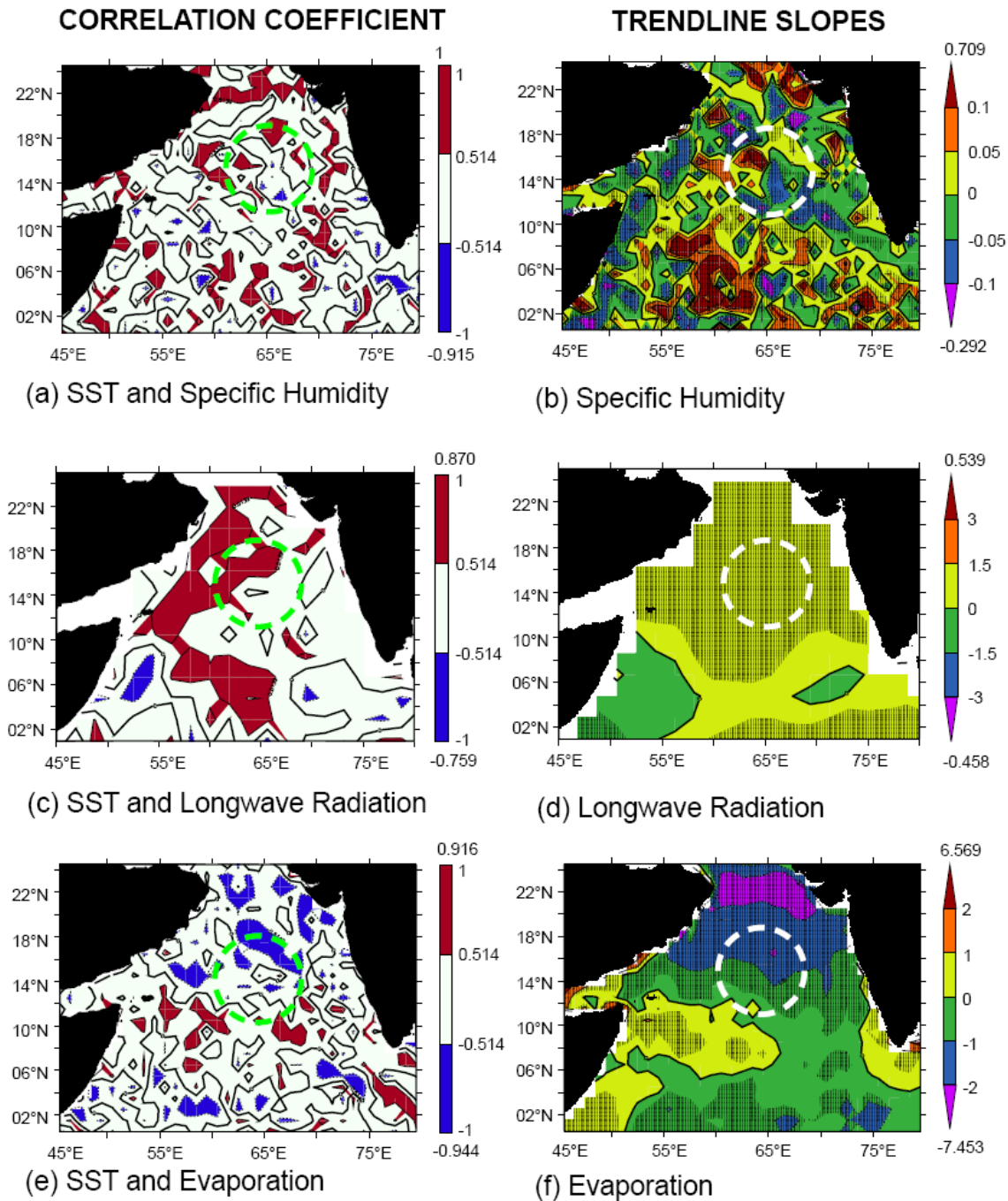


**Figure 9.** Arabian Sea fall season (October to November) averaged, correlation coefficients of SST with specific humidity (9a), longwave radiation (LWR) (9c) and evaporation (9e), coloured for regions having 95% and above significance level ( $r > |±0.514|$ ,  $N=15$ ). Spring season averaged slopes of specific humidity ((g/kg)/year) (9b), LWR ((W/m<sup>2</sup>)/year) (9d) and evaporation ((cm/year)/year) (9f), are shaded (cross-hatching) for regions having 95 % and above significance level (2-tailed t-statistic GE  $|±2.160|$ ,  $N=15$ ). LWR is considered positive into the ocean. The approximate region of highest accelerated SST warming is indicated by a dashed circle.

## SUPPLEMENTARY INFORMATION

### Processes controlling the accelerated-warming of the Arabian Sea

Joshua Rosario D'Mello<sup>†</sup> and S. Prasanna Kumar\*

CSIR- National Institute of Oceanography, Dona Paula- 403 004, Goa, India.

\*Corresponding author

email: [prasanna@nio.org](mailto:prasanna@nio.org)

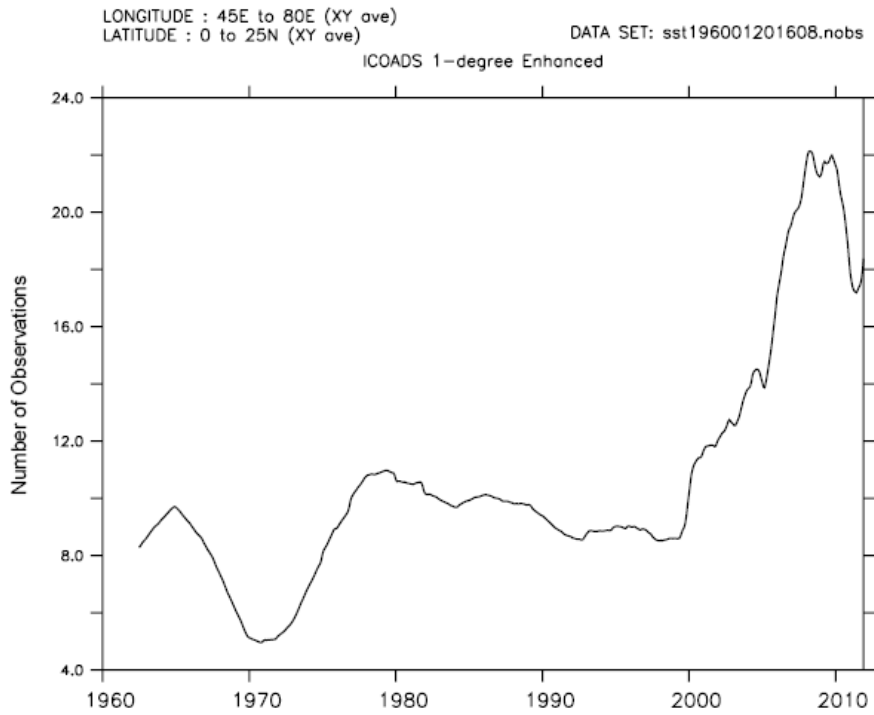
Telephone: 91-832-2450300

Fax: 91-832-2450608

<sup>†</sup> Presently at Rosary College of Commerce and Arts, Navelim- 403 707, Salcete, Goa.

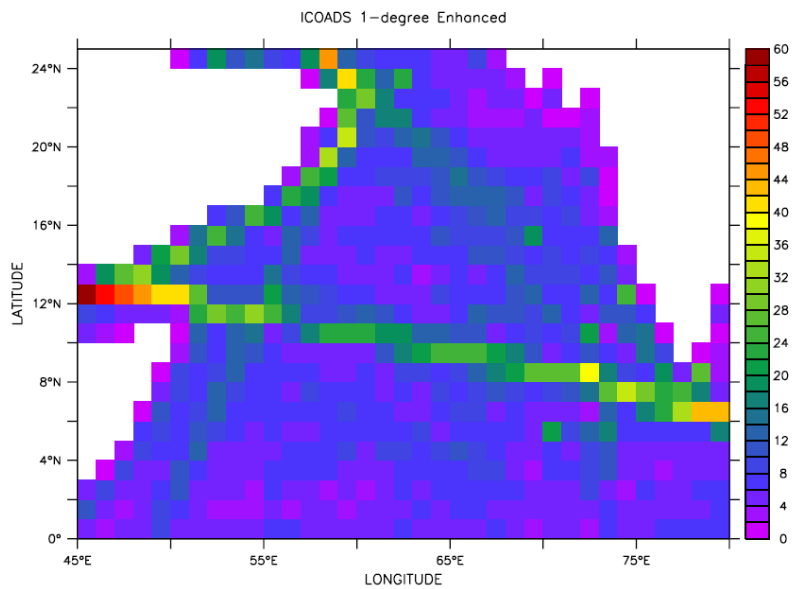
### Supplementary Information

The supplementary information contains three figures showing the quality of the International Comprehensive Ocean-Atmosphere Data-Set SST data.



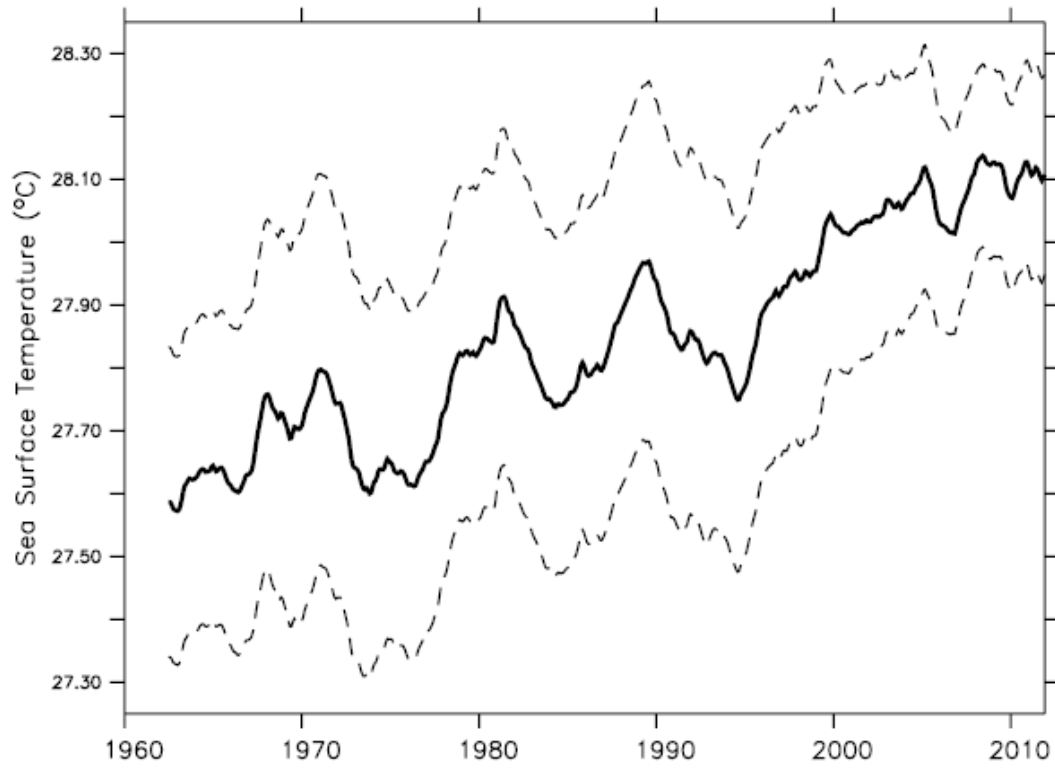
### Supplementary Figure 1.

Arabian Sea basin-averaged number of ICOADS SST observation 60-month running mean.



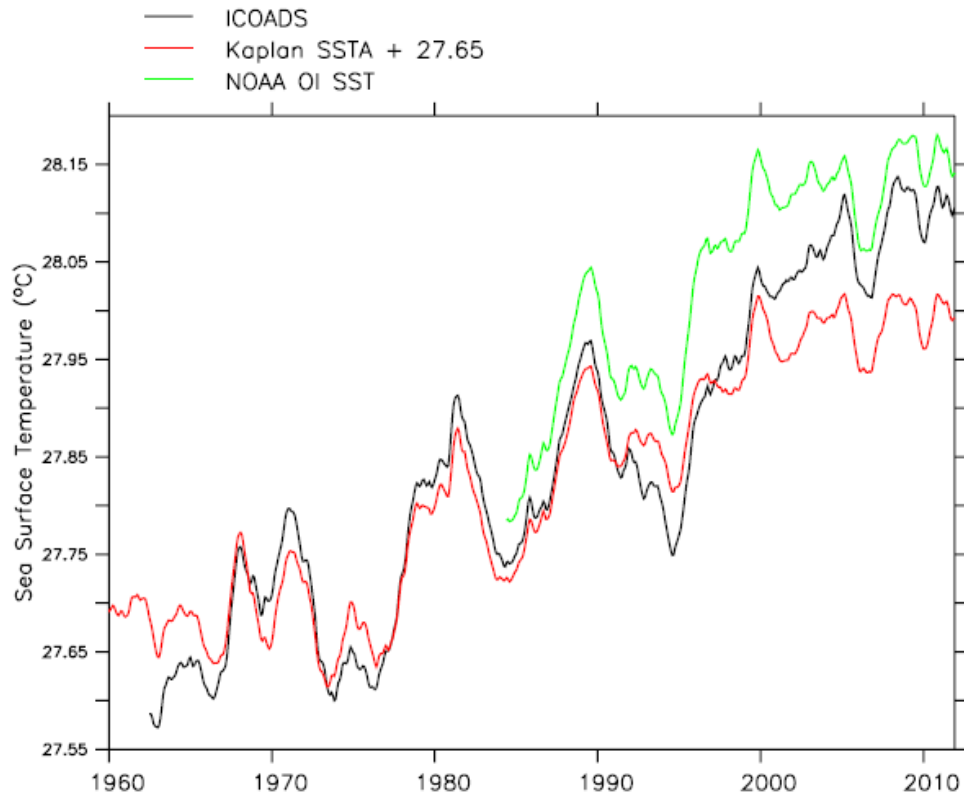
### Supplementary Figure 2.

Arabian Sea average number of monthly observations of SST, in the period from 1960 January to 2011 December



**Supplementary Figure 3.**

Arabian Sea ICOADS average SST 60-month running mean (thick black line) and the envelope of standard error (dashed lines), in the period from 1960 January to 2011



December.

#### Supplementary Figure 4.

Arabian Sea 60-month running means of ICOADS SST (black), NOAA Optimally Interpolated SST (green) and Kaplan SSTA+27.65 (red)